

Hybrid Inflation Revisited in Light of WMAP5

Mansoor Ur Rehman, Qaisar Shafi, Joshua R. Wickman

*Bartol Research Institute, Department of Physics and Astronomy,
University of Delaware, Newark, Delaware 19716, USA*

Abstract

We study the effects of including one-loop radiative corrections in a non-supersymmetric hybrid inflationary model. These corrections can arise from Yukawa couplings between the inflaton and right-handed neutrinos, and induce a maximum in the potential which admits hilltop-type solutions in addition to the standard hybrid solutions. We obtain a red-tilted spectral index n_s , consistent with WMAP5 data, for sub-Planckian values of the field. This is in contrast to the tree level hybrid analysis, in which a red-tilted spectrum is achieved only for trans-Planckian values of the field. Successful reheating is obtained at the end of the inflationary phase via conversion of the inflaton and waterfall fields into right-handed neutrinos, whose subsequent decay can explain the observed baryon asymmetry via leptogenesis.

It has been shown in the recent WMAP five year analysis (WMAP5) that tree level chaotic inflation driven by a quartic potential is excluded at the 99% confidence level [1]. The tensor to scalar ratio r in such a model turns out to be excessively large. However, this conclusion can be significantly altered provided one takes into account radiative corrections, especially those generated by any Yukawa couplings that may be present between the inflaton and fermion fields in the model. Such Yukawa couplings can be expected on general grounds, particularly in those inflation models containing right-handed neutrinos in which the observed baryon asymmetry is explained via type I leptogenesis [2]. It has been shown that radiatively improved quartic potential models with plausible values of the Yukawa couplings can yield values for r and the scalar spectral index n_s that lie well inside the $2\text{-}\sigma$ bounds provided by WMAP5 [3].

In this paper, following Ref. [3], we carry out a similar analysis for a hybrid inflationary (HI) potential [4]. In addition to providing a mechanism for generating the primordial baryon asymmetry, the extra couplings of the scalar fields in the model (especially the inflaton) to right-handed neutrinos also play an important role in how the scalars decay, and thus in the reheating of the universe. We will see that, as in the quartic case, the

radiatively corrected model explores an expanded region of parameter space, and can result in better agreement with experimental data.

At its tree level, the HI potential can be written as [5]

$$V(\chi, \phi) = \kappa^2 \left(M^2 - \frac{\chi^2}{4} \right)^2 + \frac{m^2 \phi^2}{2} + \frac{\lambda^2 \chi^2 \phi^2}{4}, \quad (1)$$

where M , m are mass parameters and κ , λ are dimensionless. The global minima of the potential lie at $(\langle \chi \rangle, \langle \phi \rangle) = (\pm 2M, 0)$. The effective mass squared of the field χ in the $\chi = 0$ direction is $m_\chi^2 = -\kappa^2 M^2 + \lambda^2 \phi^2/2$. Thus, for $\phi > \phi_c = \frac{\sqrt{2}\kappa M}{\lambda}$ the only minimum of the potential $V(\chi, \phi)$ lies at $\chi = 0$. In this region the HI potential takes the form

$$V(\phi) = V_0 + \frac{m^2 \phi^2}{2} = V_0 \left[1 + \tilde{\phi}^2 \right], \quad (2)$$

where $\tilde{\phi} \equiv \frac{m\phi}{\sqrt{2V_0}}$, and $V_0 = \kappa^2 M^4$ is the constant vacuum energy term. The second term in Eq. (2) provides a non-zero slope in the otherwise flat potential, and the system can inflate as it rolls down the $\chi = 0$ valley. Upon reaching $\phi = \phi_c$, the minimum in the χ direction becomes a maximum, and inflation ends abruptly as the system rapidly falls into the global minimum. This scenario is termed ‘‘hybrid’’ because the vacuum energy density V_0 is provided by the waterfall field χ , while ϕ is the slowly rolling inflaton field.

Before considering radiative corrections, it is appropriate to discuss the predictions of the tree level hybrid inflationary (TLHI) model in comparison with WMAP5. The slow-roll parameters for the TLHI potential are given as

$$\epsilon = \frac{m_P^2}{2} \left(\frac{\partial_\phi V}{V} \right)^2 = \frac{\eta_0}{4} \left(\frac{\partial_{\tilde{\phi}} V}{V} \right)^2 = \frac{\eta_0 \tilde{\phi}^2}{(\tilde{\phi}^2 + 1)^2}, \quad (3)$$

$$\eta = m_P^2 \left(\frac{\partial_\phi^2 V}{V} \right) = \frac{\eta_0}{2} \left(\frac{\partial_{\tilde{\phi}}^2 V}{V} \right) = \frac{\eta_0}{\tilde{\phi}^2 + 1}, \quad (4)$$

where $\eta_0 = \eta(\tilde{\phi} = 0) = \frac{m^2 m_P^2}{V_0}$, and $m_P \simeq 2.4 \times 10^{18}$ GeV is the reduced Planck mass. The number of e-foldings after the comoving scale $l_0 = 2\pi/k_0$ has crossed the horizon is given by

$$N_0 = \frac{1}{m_P^2} \int_{\phi_c}^{\phi_0} \left(\frac{V}{\partial_\phi V} \right) d\phi = \frac{2}{\eta_0} \int_{\tilde{\phi}_c}^{\tilde{\phi}_0} \left(\frac{V}{\partial_{\tilde{\phi}} V} \right) d\tilde{\phi} = \frac{1}{2\eta_0} \left(\tilde{\phi}_0^2 - \tilde{\phi}_c^2 + \ln \tilde{\phi}_0^2 / \tilde{\phi}_c^2 \right), \quad (5)$$

where ϕ_0 is the value of the field when the scale corresponding to k_0 exits the horizon, and $\phi_c = \sqrt{\frac{2\kappa}{\lambda^2}} V_0^{1/4}$ (or $\tilde{\phi}_c = \sqrt{\frac{\eta_0}{2}} (\phi_c/m_P)$), with $\kappa \sim \lambda \sim 10^{-3}$, is the value of the field at the end of inflation. In Eq. (5), we may eliminate η_0 in favor of V_0 using the curvature

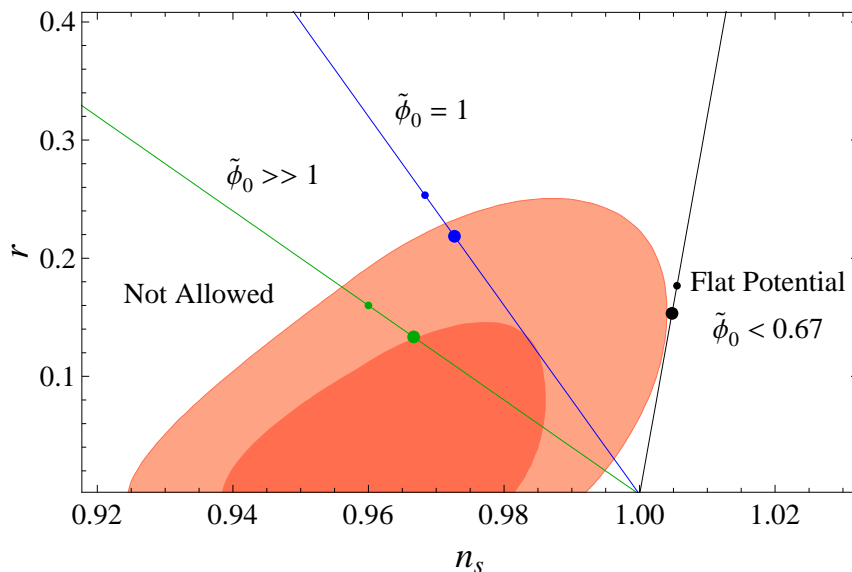


Figure 1: r vs n_s for the tree level hybrid inflationary potential, shown together with the WMAP5+BAO+SN contours (68% and 95% confidence levels) [1]. Here the small (large) dots correspond to $N_0 = 50$ ($N_0 = 60$).

perturbation constraint

$$\Delta_{\mathcal{R}} = \frac{1}{2\sqrt{3}\pi m_P^3} \frac{V^{3/2}}{|\partial_\phi V|} \Big|_{\phi=\phi_0} = \frac{1}{\sqrt{6}\eta_0\pi m_P^2} \frac{V^{3/2}}{|\partial_{\tilde{\phi}} V|} \Big|_{\tilde{\phi}=\tilde{\phi}_0} \quad (6)$$

$$\Rightarrow \eta_0 = \frac{(1 + \tilde{\phi}_0^2)^3}{24\pi^2 \Delta_{\mathcal{R}}^2 \tilde{\phi}_0^2} \left(\frac{V_0}{m_P^4} \right). \quad (7)$$

In our calculations, we will use the value $\Delta_{\mathcal{R}}(k_0) = 4.91 \times 10^{-5}$ obtained by the recent WMAP5 analysis for $k_0 = 0.002 \text{ Mpc}^{-1}$ [1]. To leading order, the spectral index n_s and the tensor-to-scalar ratio r are given by

$$n_s \simeq 1 - 6\epsilon + 2\eta = 1 - 4\eta_0 \frac{(\tilde{\phi}_0^2 - 1/2)}{(\tilde{\phi}_0^2 + 1)^2}, \quad (8)$$

$$r \simeq 16\epsilon = \frac{16\eta_0 \tilde{\phi}_0^2}{(\tilde{\phi}_0^2 + 1)^2} = 4(1 - n_s) \frac{\tilde{\phi}_0^2}{\tilde{\phi}_0^2 - 1/2}. \quad (9)$$

Using the above equations, we show in Fig. 1 the predictions of the TLHI model along with the WMAP5 1- σ and 2- σ bounds, and specify the range in which $50 < N_0 < 60$.

The flat potential regime ($\tilde{\phi}_0 \ll 1$) lies outside the $2\text{-}\sigma$ bound, corresponding to a blue spectral index. A red-tilted spectral index is obtained for $\tilde{\phi}_0 > 1/\sqrt{2} \simeq 0.71$, and for even larger values of $\tilde{\phi}_0$ this result reduces to the quadratic potential prediction $r \simeq 4(1 - n_s)$. It is interesting to study the value of the field ϕ compared to the reduced Planck mass m_P (i.e., $\phi_P \equiv \frac{\phi_0}{m_P}$) for which the spectral index is red-tilted. With $\tilde{\phi}_0 > 1/\sqrt{2}$ and the slow-roll approximation ($\eta, \epsilon \ll 1$) (which implies $\eta_0 \ll 1$), the blue spectrum can only be avoided for trans-Planckian values of the field $\phi_P = \sqrt{\frac{2}{\eta_0}} \tilde{\phi}_0 > \sqrt{\frac{1}{\eta_0}} \gg 1$. For a more exact treatment obtaining a red spectrum in the TLHI model, see the recent paper in Ref. [6]. With these tree level results in mind, we would now like to examine the situation after including radiative corrections in the HI potential.

Consider the following Lagrangian density

$$\begin{aligned} \mathcal{L} = & \frac{1}{2} \partial^\mu \phi_B \partial_\mu \phi_B + \frac{1}{2} \partial^\mu \chi_B \partial_\mu \chi_B + \frac{i}{2} \bar{N} \gamma^\mu \partial_\mu N - \kappa^2 \left(M^2 - \frac{\chi_B^2}{4} \right)^2 \\ & - \frac{m_B^2 \phi_B^2}{2} - \frac{\lambda_B^2 \chi_B^2 \phi_B^2}{4} - \frac{1}{2} y_B \phi_B \bar{N} N - \frac{1}{2} Y_B \chi_B \bar{N} N - \frac{1}{2} m_N \bar{N} N, \end{aligned} \quad (10)$$

where the subscript ‘B’ denotes bare quantities. To keep the discussion as simple as possible, we have introduced a single Yukawa coupling involving N and each of ϕ and χ . In a more realistic scenario, successful leptogenesis requires at least two right-handed neutrinos. Since $\chi = 0$ during inflation, the interaction between N and χ has no effect in this regime. After inflation, however, N acquires a contribution $M_N \simeq Y \langle \chi \rangle$ to its mass in addition to the bare mass m_N . Also, oscillations of χ affect the way in which the system reheats after inflation, as we will see later when we discuss the reheating phase.

The inflationary potential including one-loop corrections, in terms of renormalized quantities, is given by

$$V = \kappa^2 \left(M^2 - \frac{\chi^2}{4} \right)^2 + \frac{m^2 \phi^2}{2} + \frac{\lambda^2 \chi^2 \phi^2}{4} + V_{\text{loop}}, \quad (11)$$

where V_{loop} is the one-loop correction to the tree level potential. In the $\chi = 0$ direction, V_{loop} can be written as [7]

$$\begin{aligned} V_{\text{loop}} = & \frac{1}{64\pi^2} \left[m^4 \ln \left(\frac{m^2}{\mu^2} \right) + \frac{\lambda^4}{4} (\phi^2 - \phi_c^2)^2 \ln \left(\frac{\frac{\lambda^2}{2} (\phi^2 - \phi_c^2)}{\mu^2} \right) \right. \\ & \left. - 2(m_N + y\phi)^4 \ln \left(\frac{m_N + y\phi}{\mu} \right)^2 \right]. \end{aligned} \quad (12)$$

During inflation, ϕ is always larger than ϕ_c , therefore for $y\phi_c \gg (m_N, m)$ and $y \gtrsim \frac{\lambda}{\sqrt{2}}$, the above potential reduces to

$$V_{\text{loop}} = -A\phi^4 \ln \left(\frac{y\phi}{\mu} \right), \quad \text{with } A = \frac{y^4}{16\pi^2}. \quad (13)$$

In order to ensure that the log factor is always positive during inflation, it is convenient to set the renormalization scale at $\mu = y \phi_c$. Then, the complete radiatively-corrected hybrid inflationary (RCHI) potential in the $\chi = 0$ direction reduces to the form

$$V = V_0 + \frac{m^2 \phi^2}{2} - A_\phi \phi^4 = V_0 \left[1 + \tilde{\phi}^2 - \tilde{A}_\phi \tilde{\phi}^4 \right], \quad (14)$$

where $\tilde{A}_\phi = \frac{4A_\phi}{\eta_0^2 (V_0/m_P^4)}$ and $A_\phi = A \ln\left(\frac{\phi}{\phi_c}\right)$. In the following calculations, we will approximate \tilde{A}_ϕ to be independent of ϕ . The slow-roll parameters in this case are given by

$$\epsilon = \frac{\eta_0 \left(\tilde{\phi} - 2 \tilde{A}_\phi \tilde{\phi}^3 \right)^2}{\left(1 + \tilde{\phi}^2 - \tilde{A}_\phi \tilde{\phi}^4 \right)^2}, \quad \eta = \frac{\eta_0 \left(1 - 6 \tilde{A}_\phi \tilde{\phi}^2 \right)}{1 + \tilde{\phi}^2 - \tilde{A}_\phi \tilde{\phi}^4}. \quad (15)$$

Using Eq. (6) and solving for η_0 as before, we find

$$\eta_0 = \frac{\left(1 + \tilde{\phi}_0^2 - \tilde{A}_\phi \tilde{\phi}_0^4 \right)^3}{24 \pi^2 \Delta_{\mathcal{R}}^2 \tilde{\phi}_0^2 \left(1 - 2 \tilde{A}_\phi \tilde{\phi}_0^2 \right)^2} \left(\frac{V_0}{m_P^4} \right). \quad (16)$$

The number of e-foldings in the RCHI model can be calculated as

$$N_0 = \frac{1}{2\eta_0} \left(\frac{\tilde{\phi}_0^2 - \tilde{\phi}_c^2}{2} + \ln \frac{\tilde{\phi}_0^2}{\tilde{\phi}_c^2} - \frac{\left(1 + 4 \tilde{A}_\phi \right) \ln \left[\frac{1 - 2 \tilde{A}_\phi \tilde{\phi}_0^2}{1 - 2 \tilde{A}_\phi \tilde{\phi}_c^2} \right]}{4 \tilde{A}_\phi} \right). \quad (17)$$

In order to ensure that the potential remains bounded during inflation, we take $\tilde{\phi}_c < \tilde{\phi}_0 < \tilde{\phi}_M = \frac{1}{\sqrt{2 \tilde{A}_\phi}}$, where $\tilde{\phi}_M$ is field value at the maximum of the potential. This maximum introduces hilltop-type solutions [8], to which we now turn our discussion.

In its approximate form, the potential in Eq. (14) has previously been analyzed only for sub-Planckian hilltop-type solutions [9], for which inflation begins in a region where the potential is concave downward. In general, the RCHI model can lead to both hilltop and non-hilltop solutions (see Ref. [3] for a similar analysis in the case of radiatively-corrected quadratic and quartic potentials). In order to study both types of solutions, it will be convenient to define the quantities $f \equiv \tilde{\phi}_0/\tilde{\phi}_M$, $f_c \equiv \tilde{\phi}_c/\tilde{\phi}_M$ and $f_1 \equiv \sqrt{2 \tilde{A}_\phi}$. As we will see, for the same values of \tilde{A}_ϕ and V_0 , we can always distinguish two separate branches of solutions, one with large f values and another with small f values. To facilitate our discussion, we can rewrite the number of e-foldings in the form

$$N_0 = \frac{1}{2\eta_0} \times \left(\frac{f^2 - f_c^2}{2 f_1^2} + \ln \frac{f^2}{f_c^2} + \frac{(f_1^2 + 1/2)}{f_1^2} \ln \frac{1 - f_c^2}{1 - f^2} \right), \quad (18)$$

where

$$f_c = f_1 \left(\frac{V_0^{1/4}}{m_P} \right) \sqrt{\frac{2\eta_0}{y}}, \quad \eta_0 = \frac{V_0/m_P^4}{24 \pi^2 \Delta_{\mathcal{R}}^2} \left(\frac{\left(1 + (f/f_1)^2 (1 - f^2/2) \right)^3}{(f/f_1)^2 (1 - f^2)^2} \right). \quad (19)$$

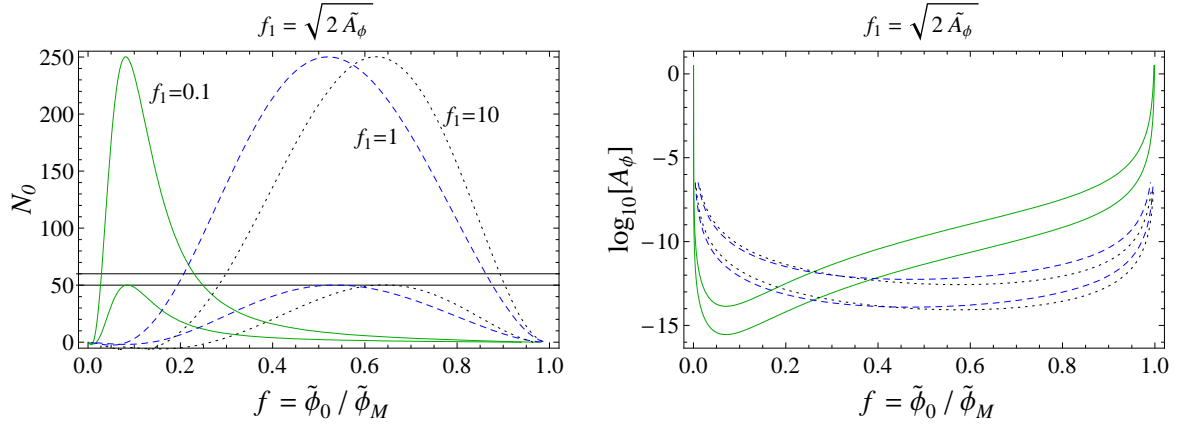


Figure 2: N_0 and $\log_{10}[A_\phi]$ vs f for $f_1 = 0.1, 1$ and 10 with $V_0^{1/4} = (10^{16.15} - 10^{16.29})$ GeV, $(10^{16.08} - 10^{16.22})$ GeV and $(10^{15.61} - 10^{15.74})$ GeV respectively. We obtain two solutions (n_s, r) for each value of A_ϕ and V_0 .

In order to discuss the two branches qualitatively, we note that the factor inside parentheses in N_0 is slowly varying over the entire range of f . Therefore, it is sufficient to consider only the contribution of the η_0^{-1} factor in N_0 . For large values of f_1 , η_0^{-1} reduces to the form $f^2(1-f^2)^2$, with a maximum at $f = 1/\sqrt{3} \sim 0.58$. As we move away from this maximum, we obtain the same value of N_0 for each of two values of f , one smaller and one larger than $1/\sqrt{3}$. These large- f and small- f branches can be seen in Fig. 2. As f_1 is lowered, the maximum of N_0 moves toward smaller values of f , asymptotically tending toward $f = f_1/\sqrt{2}$.

Let us discuss in greater detail the large f_1 limit, which corresponds to the ‘‘flat potential regime’’ (i.e. $\tilde{\phi}_0 = f/f_1 \ll 1$). In this limit, the number of e-foldings N_0 reduces to

$$N_0 \simeq \frac{12 \pi^2 \Delta_{\mathcal{R}}^2}{V_0/m_P^4} \left(\frac{f^2(1-f^2)^2}{f_1^2} \right) \ln \frac{f_c^2(1-f_c^2)}{f^2(1-f^2)}, \quad (20)$$

with

$$f_c \simeq \sqrt{\frac{1}{12 y \pi^2 \Delta_{\mathcal{R}}^2} \left(\frac{V_0^{1/4}}{m_P} \right)^3 \left(\frac{f_1^2}{f^2(1-f^2)} \right)} f. \quad (21)$$

An upper bound on V_0 can be found by considering the point at which the two branches meet for a given value of f_1 . Owing to the inverse dependence of N_0 on V_0 , the number of e-foldings at the maximum is shifted upward as V_0 is decreased away from its limiting value, and the two branches diverge from one another in the range corresponding to realistic values of N_0 . The basic condition $f > f_c$ (or $N_0 > 0$) leads to the bound $V_0^{1/4} \lesssim \frac{3 \times 10^{16}}{f_1^{2/3}}$

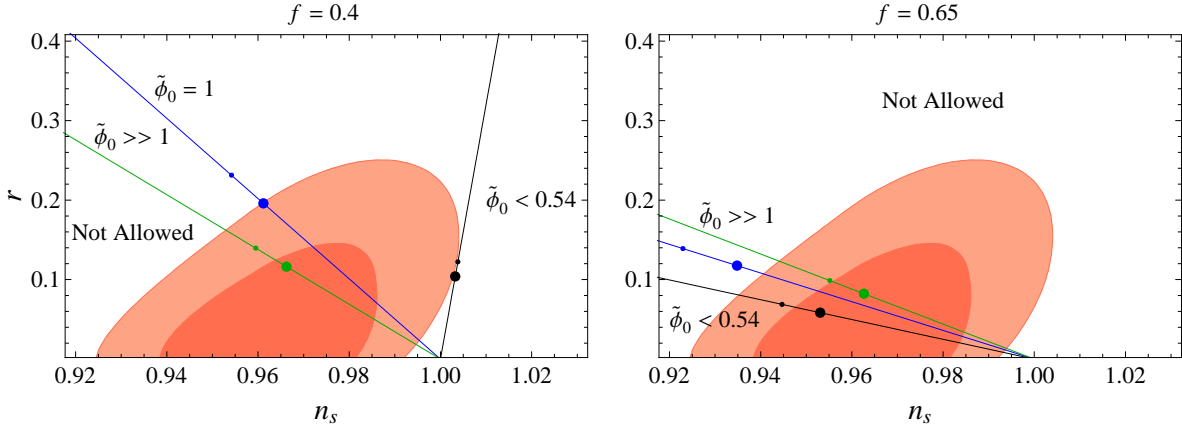


Figure 3: r vs n_s for radiatively-corrected hybrid inflation, with $f = 0.4$ and $f = 0.65$. Here, small (large) dots correspond to $N_0 = 50$ ($N_0 = 60$). Compared to Fig. 1, smaller values of $\tilde{\phi}_0$ fall within the WMAP5 bounds. In addition, the allowed and disallowed regions are exchanged in going from a non-hilltop ($f < f_i$) to a hilltop ($f > f_i$) solution.

GeV. In order to obtain a realistic number of e-foldings, V_0 must obey a somewhat more stringent bound.

As mentioned earlier, hilltop solutions are defined as having a concave downward curvature of the potential when inflation begins. Therefore, only those solutions which satisfy $f \gtrsim f_i = 1/\sqrt{3} \simeq 0.58$ will be called hilltop solutions, where f_i is the value of f at the point of inflection.

The spectral index n_s and the tensor-to-scalar ratio r for the RCHI model are given as

$$n_s = 1 + 2\eta_0 \frac{\left(1 - 2(1 + 3\tilde{A}_\phi)\tilde{\phi}_0^2 + 5\tilde{A}_\phi\tilde{\phi}_0^4 - 6\tilde{A}_\phi^2\tilde{\phi}_0^6\right)}{\left(1 + \tilde{\phi}_0^2 - \tilde{A}_\phi\tilde{\phi}_0^4\right)^2}, \quad (22)$$

$$r = \frac{16\eta_0 \left(\tilde{\phi}_0 - 2\tilde{A}_\phi\tilde{\phi}_0^3\right)^2}{\left(1 + \tilde{\phi}_0^2 - \tilde{A}_\phi\tilde{\phi}_0^4\right)^2} = 4(1 - n_s) \frac{\tilde{\phi}_0^2 (1 - f^2)^2}{\tilde{\phi}_0^2 \left(1 - \frac{5}{4}f^2 + \frac{3}{4}f^4\right) - \frac{1}{2} \left(1 - \frac{3}{2}f^2\right)}. \quad (23)$$

The spectral index becomes unity when $\tilde{\phi}_0$ acquires the value

$$\tilde{\phi}_0 = \frac{1}{\sqrt{2}} \left(\frac{\sqrt{1 - 3f^2}}{\sqrt{1 - \frac{5}{4}f^2 + \frac{3}{4}f^4}} \right), \quad (24)$$

which reduces to the tree level result $\tilde{\phi}_0 = \frac{1}{\sqrt{2}}$ in the $f \rightarrow 0$ limit. For $\tilde{\phi}_0$ values larger

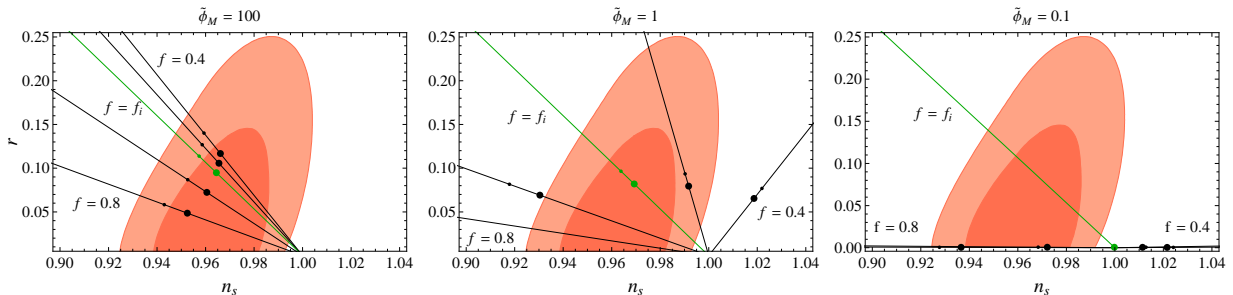


Figure 4: r vs n_s for radiatively-corrected hybrid inflation, with $\tilde{\phi}_M = 100, 1$ and 0.1 for $f = 0.4, 0.5, f_i, 0.7$ and 0.8 . Large values of $\tilde{\phi}_M$ result in appreciable values of r for a realistic number of e-foldings.

(smaller) than in Eq. (24), we obtain a red-tilted (blue-tilted) spectral index if $f < f_i$. For $f > f_i$, η becomes negative and we always have a red-tilted spectral index.

For small values of f , Eq. (23) reduces to the tree level result $r \simeq 4(1 - n_s) \frac{\tilde{\phi}_0^2}{\tilde{\phi}_0^2 - 1/2}$.

Similarly, for large values of $\tilde{\phi}_0$ we find $r \simeq 4(1 - n_s) \frac{(1-f^2)^2}{(1-\frac{5}{4}f^2+\frac{3}{4}f^4)}$, which reduces to the quadratic prediction $r \simeq 4(1 - n_s)$ in the small f limit (see Figs. 3 and 4). Thus we see that in order for the radiative corrections to produce a reasonably large contribution, $\tilde{\phi}_0$ should be chosen close to $\tilde{\phi}_M$. This choice in turn shifts the “flat potential regime” toward the inside of the $2\text{-}\sigma$ bound of the WMAP+BAO+SN data, as can be seen by comparing Figs. 1 and 3. A larger choice of f leads to a greater portion of the “flat” region inside the bounds. Additionally, Fig. 3 shows that for $f < f_i$ the allowed regime lies above the $\tilde{\phi}_0 = 100$ line, whereas for $f > f_i$ the allowed regime lies below this line. As noted earlier, for $f > f_i$, η becomes negative and both ϵ and η tend to drive n_s ($\simeq 1 - 6\epsilon + 2\eta$) below 1 as η_0 increases. In contrast, for $f < f_i$, η is always positive and competes with ϵ , allowing n_s values above or somewhat below 1.

In our discussion so far, we have suppressed the ϕ dependence of A_ϕ in order to obtain analytically tractable expressions. Next, we employ numerical calculations to examine the RCHI model in such a way that this dependence can be taken into account. In these calculations, we use the next-to-leading order expressions for n_s , r , and $\Delta_{\mathcal{R}}$ for added precision [12]. Having already explored the relative behavior of the quadratic and vacuum terms, we will use the form of the potential Eq. (14) written in terms of ϕ rather than $\tilde{\phi}$ in order to more directly probe the parameters m^2 and V_0 .

As discussed earlier, inflation ends via a waterfall effect at the critical value ϕ_c . It is worth noting that inflation can end due to the breakdown of the slow-roll approximation, before ϕ reaches this value; however, in our calculations below, $|\eta| \lesssim 10^{-2}$ and $\epsilon \lesssim 10^{-5}$ when evaluated at ϕ_c , and so the slow-roll relations are still valid when the waterfall is induced.

In terms of the reheat temperature T_r , the number of observable e-foldings may be written as [10]

$$N_0 \simeq 53 + \frac{2}{3} \ln \left[\frac{V(\phi_0)^{1/4}}{10^{15} \text{ GeV}} \right] + \frac{1}{3} \ln \left[\frac{T_r}{10^9 \text{ GeV}} \right], \quad (25)$$

where $T_r \simeq \left[\frac{30/g_*}{2\pi^3(1+w_{reh})(5-3w_{reh})} \right]^{1/4} \sqrt{\Gamma m_P}$ [11], and Γ is some appropriate decay width. Two sources of primordial N production contribute to reheating, resulting from the oscillations of ϕ and χ about their respective minima. The decay rates of these two processes are given by

$$\Gamma_{\chi \rightarrow NN} = \frac{Y^2 m_\chi}{8\pi}, \quad \Gamma_{\phi \rightarrow NN} = \frac{y^2 m_\phi}{8\pi}, \quad (26)$$

where $Y \simeq M_N/\langle\chi\rangle$, and the scalar field masses are given as

$$m_\chi = \sqrt{2} \kappa M, \quad m_\phi = \sqrt{m^2 + 2(\lambda M)^2}. \quad (27)$$

To see how these two contributions compare, consider the ratio of their decay rates

$$\frac{\Gamma_{\phi \rightarrow NN}}{\Gamma_{\chi \rightarrow NN}} = \left(\frac{y}{Y} \right)^2 \frac{m_\phi}{m_\chi}. \quad (28)$$

To simplify the analysis, we will take $\lambda \sim \kappa \sim y \sim Y$. Then, for $m \ll M$, we obtain $m_\phi \sim m_\chi$ and the ratio of the decay rates in Eq. (28) is of order unity. Indeed, under these assumptions, it turns out that all relevant decay widths are of the same order, and

f	$V_0^{1/4}$ (GeV)	A (10^{-13})	M (GeV)	m (GeV)	f_c	n_s	r (10^{-3})	m_ϕ (10^{14} GeV)	T_r (10^{12} GeV)	N_0
$\phi_P = 0.25$										
0.65	3.696×10^{15}	1.164	5.744×10^{16}	9.04×10^{11}	0.1735	0.9864	0.149	1.68	1.45	56.30
0.70	3.584×10^{15}	1.282	5.503×10^{16}	8.74×10^{11}	0.1789	0.9717	0.132	1.65	1.47	56.29
0.75	3.434×10^{15}	1.336	5.245×10^{16}	8.29×10^{11}	0.1828	0.9536	0.111	1.59	1.46	56.25
0.80	3.235×10^{15}	1.296	4.960×10^{16}	7.63×10^{11}	0.1843	0.9312	0.0870	1.49	1.41	56.19
$\phi_P = 1$										
0.60	8.873×10^{15}	2.134	1.278×10^{17}	6.13×10^{12}	0.08907	0.9930	5.02	4.36	2.72	57.10
0.65	8.603×10^{15}	2.333	1.225×10^{17}	5.87×10^{12}	0.09252	0.9768	4.43	4.27	2.75	57.08
0.70	8.262×10^{15}	2.430	1.171×10^{17}	5.53×10^{12}	0.09521	0.9575	3.77	4.12	2.73	57.04
0.75	7.836×10^{15}	2.387	1.113×10^{17}	5.10×10^{12}	0.09696	0.9346	3.04	3.90	2.65	56.99
$\phi_P = 2.5$										
0.55	1.482×10^{16}	2.280	2.116×10^{17}	1.88×10^{13}	0.05409	0.9921	43.1	7.34	3.59	57.55
0.60	1.443×10^{16}	2.549	2.032×10^{17}	1.81×10^{13}	0.05665	0.9783	38.7	7.24	3.67	57.53
0.65	1.394×10^{16}	2.728	1.947×10^{17}	1.72×10^{13}	0.05880	0.9619	33.7	7.06	3.68	57.50
0.70	1.334×10^{16}	2.779	1.859×10^{17}	1.60×10^{13}	0.06046	0.9427	28.2	6.77	3.62	57.48

Table 1: Predicted values of various inflationary parameters in the radiatively-corrected hybrid model. Here we show only those values falling within the WMAP5+BAO+SN 2σ bounds (see Fig. 6) for each of the three cases $\phi_P \equiv \frac{\phi_0}{m_P} = 0.25, 1, \text{ and } 2.5$, which correspond primarily to hilltop solutions ($f \gtrsim 0.6$). These values correspond to the choice $\phi_c \simeq 2V_0^{1/4}/\sqrt{y}$ in Eq.(30).

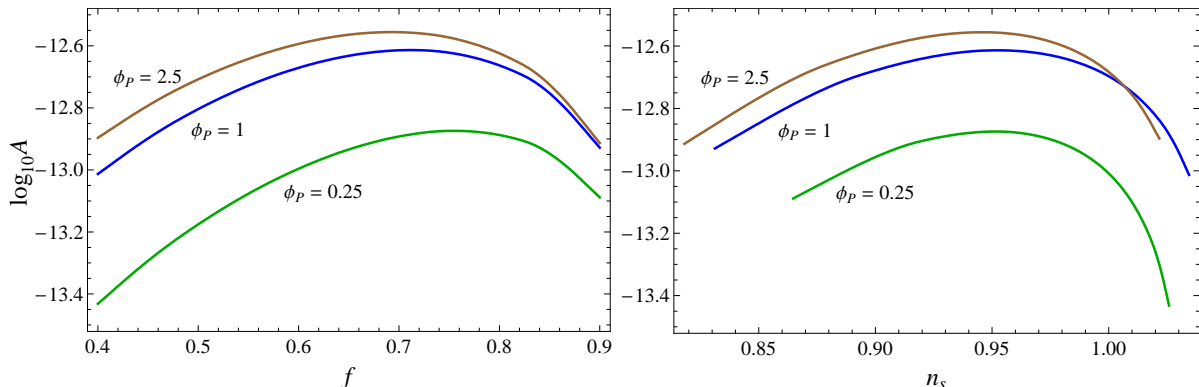


Figure 5: $\log_{10} A$ vs. f and n_s for the cases $\phi_P \equiv \frac{\phi_0}{m_P} = 0.25, 1, \text{ and } 2.5$. Two solutions of each of f, n_s exist for a single value of A (see Fig. 2). The region falling within the WMAP5 bounds mainly leads to two hilltop solutions.

so we may approximate the total decay width appearing in T_r as $\Gamma \sim \Gamma_{\phi \rightarrow NN}$. Then, using $w_{reh} = 0$ for matter dominant reheating and taking $g_* \simeq 106$, the reheat temperature becomes $T_r \simeq 0.035 y \sqrt{m_\phi m_P}$.

To proceed further, we may eliminate m^2 in favor of the field value at the local maximum ϕ_M induced by the radiative correction term. Assuming this maximum is the only extremum other than the minimum at the origin, we can write

$$m^2 = A\phi_M^2 \left(1 + 4 \ln \frac{\phi_M}{\phi_c} \right). \quad (29)$$

Using the approximations above, we may simplify the expression for the critical value of the inflaton field:

$$\phi_c = \sqrt{\frac{2\kappa}{\lambda^2}} V_0^{1/4} \sim \frac{V_0^{1/4}}{\sqrt{y}}. \quad (30)$$

Note that this expression depends only on V_0 and A (via y).

We are interested in comparing sub-Planckian and trans-Planckian inflation. We thus consider three values of the inflaton at the start of inflation: $\phi_P = 0.25, \phi_P = 1$ and $\phi_P = 2.5$. In each of these cases, if the ratio f is fixed, ϕ_M is known and the inflationary potential $V(\phi)$ is specified in terms of V_0 and A .

To perform our numerical calculations, we fix a value of f and scan over values of V_0 until the number of e-foldings N_0 given by an integral similar to Eq. (5) matches its value as given by thermal considerations, Eq. (25). For each (ϕ_0, f, V_0) , the value of A can then be calculated by setting the curvature perturbation equal to its WMAP5 value. The results of these calculations are displayed in Table 1.

The RCHI model yields values of the reheat temperature on the order of $T_r \sim 10^{12}$ GeV, which is substantially larger than the range allowed by supersymmetric models of inflation,

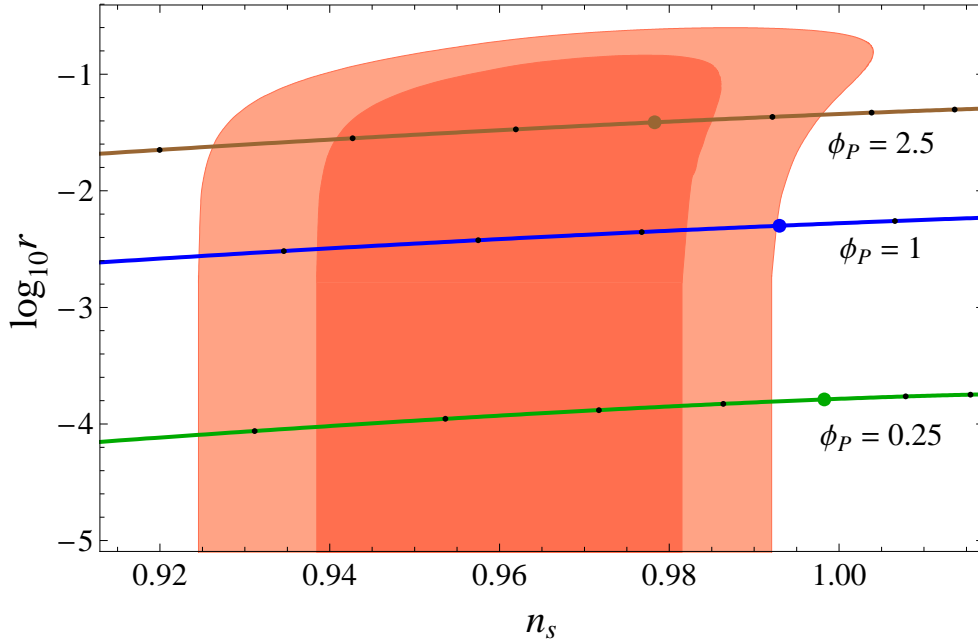


Figure 6: $\log_{10} r$ vs. n_s for the cases $\phi_P \equiv \frac{\phi_0}{m_P} = 0.25, 1, \text{ and } 2.5$, shown together with the WMAP5+BAO+SN contours. The smaller black dots denote f values increasing from right to left in increments of 0.05, and the larger colored dots represent inflation starting at the inflection point of the potential, with $f_i \approx 0.60$. With larger values of ϕ_P , the WMAP5 limit on r can be saturated.

$T_r \sim 10^6\text{-}10^9$ GeV [13]. This range is formulated based on the gravitino constraint, which is peculiar to susy models and does not pose a danger to the non-susy model that we currently consider. Table 1 also shows that, in order to obtain a spectral index near the WMAP5 central value, the RCHI model predicts $V_0^{1/4} \sim 10^{15}\text{-}10^{16}$ GeV. A similar range of preferred $V_0^{1/4}$ values has recently been realized in other models such as susy hybrid inflation [14] and non-susy Coleman-Weinberg and Higgs inflation [15]. In the non-susy models, this range was also seen to be associated with proton decay, predicting a lifetime of $10^{34}\text{-}10^{38}$ years. In addition, such models predict a reheat temperature 4-6 orders of magnitude lower than the RCHI model, due in part to a Yukawa coupling on the order of 10^{-6} . In contrast, the Yukawa coupling involving ϕ in the RCHI model is linked to the coefficient $A \sim 10^{-13}$, implying $y \sim 10^{-3}$.

Fig. 5 shows the behavior of A with respect to both f and n_s in each of our three cases. Each value of A corresponds to two solutions of f and n_s , as expected based on our previous calculations. Given our current choice of fixed parameters, some values of A result in one hilltop solution and one non-hilltop solution, while others result in two hilltop solutions. In the numerical case, the value of f_i deviates somewhat from its approximate analytical value $1/\sqrt{3}$, hovering close to 0.60 for all three cases.

The results of our numerical calculations for the RCHI model are compared to WMAP5

in Fig. 6. As f increases along the curves of constant ϕ_P , n_s decreases to values less than unity. If f is increased further, these curves pass into the region favored by WMAP5, span the full $2\text{-}\sigma$ range, and pass outside the bounds again. For the values of ϕ_P which we have considered, we obtain a favored range of f corresponding to $0.55 \lesssim f \lesssim 0.80$. Stated differently, the inclusion of suitable radiative correction effects in the HI scenario results in the model becoming more favored by the WMAP5 data.

In the range $0.4 \leq f \leq 0.9$ that we have explored, each choice of ϕ_0 produces a distinct prediction for the size of r . The case $\phi_P = 2.5$, which admits trans-Planckian values of the inflaton, results in an appreciable value of r while the others predict a vanishingly small value. Future missions such as PLANCK may be capable of measuring this quantity with far greater precision.

Summary

We obtain a scalar spectral index n_s consistent with WMAP5 data by including fermion-dominated one-loop radiative corrections in a non-susy hybrid inflationary model. A compelling candidate for the origin of these corrections is a Yukawa coupling involving the inflaton and right-handed neutrinos. A red-tilted spectral index is obtained for sub-Planckian values of the inflaton field, which was excluded to $2\text{-}\sigma$ by WMAP5 in the case of the tree level hybrid model. Furthermore, these corrections make accessible both non-hilltop and hilltop-type solutions in this model, and a red-tilted spectrum is achieved primarily for hilltop solutions.

Acknowledgments

We thank Nefer Şenoğuz for valuable discussions. This work is supported in part by the DOE under grant # DE-FG02-91ER40626 (Q.S. and M.R.), by the Bartol Research Institute (M.R.), and by the NSF under grant # DGE 0538555 (J.W.).

References

- [1] E. Komatsu *et al.* [WMAP Collaboration], arXiv:0803.0547 [astro-ph].
- [2] M. Fukugita and T. Yanagida, Phys. Lett. B **174**, 45 (1986); G. Lazarides and Q. Shafi, Phys. Lett. B **258**, 305 (1991), for non-thermal leptogenesis.
- [3] V. Nefer Senoguz and Q. Shafi, Phys. Lett. B **668**, 6 (2008) [arXiv:0806.2798 [hep-ph]].
- [4] A. D. Linde, Phys. Lett. B **259**, 38 (1991); A. D. Linde, Phys. Rev. D **49**, 748 (1994) [arXiv:astro-ph/9307002].
- [5] For a review and additional references, see G. Lazarides, Lect. Notes Phys. **592**, 351 (2002) [arXiv:hep-ph/0111328].

- [6] S. Clesse and J. Rocher, arXiv:0809.4355 [hep-ph].
- [7] S. R. Coleman and E. J. Weinberg, Phys. Rev. D **7**, 1888 (1973). For a review and additional references, see M. Sher, Phys. Rept. **179**, 273 (1989).
- [8] L. Boubekeur and D. H. Lyth, JCAP **0507**, 010 (2005) [arXiv:hep-ph/0502047].
- [9] K. Kohri, C. M. Lin and D. H. Lyth, JCAP **0712**, 004 (2007) [arXiv:0707.3826 [hep-ph]]; C. M. Lin and K. Cheung, arXiv:0901.3280 [hep-ph].
- [10] A. R. Liddle and S. M. Leach, Phys. Rev. D **68**, 103503 (2003) [arXiv:astro-ph/0305263].
- [11] J. Martin and C. Ringeval, JCAP **0608**, 009 (2006) [arXiv:astro-ph/0605367]; A. Linde, *Particle Physics and Inflationary Cosmology* (Harwood Academic Publishers, 1990); E.W. Kolb and M.S. Turner, *The Early Universe* (Westview, 1990); A.R. Liddle and D.H. Lyth, *Cosmological Inflation and Large-Scale Structure* (Cambridge, 2000).
- [12] E. D. Stewart and D. H. Lyth, Phys. Lett. B **302**, 171 (1993) [arXiv:gr-qc/9302019].
- [13] V. N. Senoguz and Q. Shafi, Phys. Rev. D **71**, 043514 (2005) [arXiv:hep-ph/0412102] and references therein.
- [14] G. R. Dvali, Q. Shafi and R. K. Schaefer, Phys. Rev. Lett. **73**, 1886 (1994) [arXiv:hep-ph/9406319]; E. J. Copeland, A. R. Liddle, D. H. Lyth, E. D. Stewart and D. Wands, Phys. Rev. D **49**, 6410 (1994) [arXiv:astro-ph/9401011]; G. Lazarides, R. K. Schaefer and Q. Shafi, Phys. Rev. D **56**, 1324 (1997) [arXiv:hep-ph/9608256]; A. D. Linde and A. Riotto, Phys. Rev. D **56**, 1841 (1997) [arXiv:hep-ph/9703209]; R. Jeannerot, S. Khalil, G. Lazarides and Q. Shafi, JHEP **0010**, 012 (2000) [arXiv:hep-ph/0002151]; B. Garbrecht, C. Pallis and A. Pilaftsis, JHEP **0612**, 038 (2006) [arXiv:hep-ph/0605264]; M. Bastero-Gil, S. F. King and Q. Shafi, Phys. Lett. B **651**, 345 (2007) [arXiv:hep-ph/0604198]; M. ur Rehman, V. N. Senoguz and Q. Shafi, Phys. Rev. D **75**, 043522 (2007) [arXiv:hep-ph/0612023]; C. Pallis, arXiv:0710.3074 [hep-ph].
- [15] M. U. Rehman, Q. Shafi and J. R. Wickman, Phys. Rev. D **78**, 123516 (2008) [arXiv:0810.3625 [hep-ph]]; R. Kallosh and A. Linde, JCAP **0704**, 017 (2007) [arXiv:0704.0647 [hep-th]].